Earth and Planetary Science Letters 400 (2014) 292–301

Contents lists available at ScienceDirect

Earth and Planetary Science Letters

www.elsevier.com/locate/epsl

Distribution of discrete seismic asperities and aseismic slip along the Ecuadorian megathrust

M. Chlieh [a,*], P.A. Mothes [b], J.-M. Nocquet [a], P. Jarrin [b], P. Charvis [a], D. Cisneros [c], Y. Font [a], J.-Y. Collot [a], J.-C. Villegas-Lanza [d], F. Rolandone [e], M. Vallée [f], M. Regnier [a], M. Segovia [b], X. Martin [a], H. Yepes [b]

[a] Géoazur, Université Nice Sophia Antipolis, IRD, CNRS, OCA, Nice, France
[b] Instituto Geofísico, Escuela Politécnica Nacional, Quito, Ecuador
[c] Instituto Geográfico Militar, Quito, Ecuador
[d] Instituto Geofísico del Perú, Lima, Peru
[e] Université Pierre et Marie Curie, Paris, France
[f] Institut de Physique du Globe de Paris, Sorbonne Paris Cité, Univ. Paris Diderot, UMR 7154 CNRS, 75005 Paris, France

ARTICLE INFO

Article history:
Received 16 January 2014
Received in revised form 11 May 2014
Accepted 14 May 2014
Available online xxxx
Editor: P. Shearer

Keywords:
Ecuador–Colombia subduction zone
interseismic coupling models
seismic asperities
large and great megathrust earthquakes
slow slip event
aseismic slip

ABSTRACT

A dense GPS network deployed in Ecuador reveals a highly heterogeneous pattern of interseismic coupling confined in the first 35 km depth of the contact between the subducting oceanic Nazca plate and the North Andean Sliver. Interseismic models indicate that the coupling is weak and very shallow (0–15 km) in south Ecuador and increases northward, with maximum found in the rupture areas of large (Mw > 7.0) megathrust earthquakes that occurred during the 20th century. Since the great 1906 Mw = 8.8 Colombia–Ecuador earthquake may have involved the simultaneous rupture of three to six asperities, only one or two asperities were reactivated during the large seismic sequence of 1942 (Mw = 7.8), 1958 (Mw = 7.7), 1979 (Mw = 8.2) and 1998 (Mw = 7.1). The axis of the Carnegie Ridge, which is entering the subduction zone south of the Equator, coincides well with the location of a 50 km wide creeping corridor that may have acted as persistent barrier to large seismic ruptures. South of this creeping region, a highly locked asperity is found right below La Plata Island. While this asperity may have the potential to generate an Mw ~ 7.0–7.5 earthquake and a local tsunami, until now it is unknown to have produced any similar events. That region is characterized by the presence of slow slip events that may contribute significantly to reduce the long-term moment deficit accumulated there and postpone the failure of that asperity. At the actual accumulation rate, a characteristic recurrence time for events such as those in 1942, 1958 and 1979 is 140 ± 30 yr, 90 ± 20 yr, 153 ± 80 yr respectively. For the great 1906 event, we find a recurrence time of at least 575 ± 100 yr, making the great 1906 earthquake a rare super cycle event.

1. Introduction

Fast subduction of the oceanic Nazca plate beneath the South American continental plate provokes large (Mw > 7.5) megathrust earthquakes with a characteristic return time of 100–250 yr (Nishenko, 1991). The Ecuador–Colombia subduction zone has experienced five large megathrust earthquakes during the 20th century (Beck and Ruff, 1984; Kanamori and McNally, 1982; Swenson and Beck, 1996). From central Ecuador to north Colombia, megathrust earthquakes occurred in 1942 (Mw = 7.8), 1958 (Mw = 7.7), 1979 (Mw = 8.2) and 1998 (Mw = 7.1) within the 500-km long rupture area of the great 1906 (Mw = 8.8) Colombia–Ecuador earthquake (Figs. 1 and 2). The variation in the mode of rupture of the 1906 segment is one of the classical examples that led seismologists to introduce the concept of the asperity model to describe some of the complexities in the successive mode of rupture of a given subduction segment (Kanamori and McNally, 1982; Lay et al., 1989; Thatcher, 1990). Within this model, the megathrust interface is supposedly creeping nearly everywhere except at major large asperities or group of smaller size asperities that are heterogeneously distributed along the megathrust seismogenic zone. These asperities concentrate a moment deficit that is slowly increasing during the interseismic periods and ultimately released through large megathrust earthquakes. Although that initial conceptualization of

* Corresponding author.
E-mail addresses: chlieh@geoazur.unice.fr, mohamed.chlieh@ird.fr (M. Chlieh).

http://dx.doi.org/10.1016/j.epsl.2014.05.027
0012-821X/

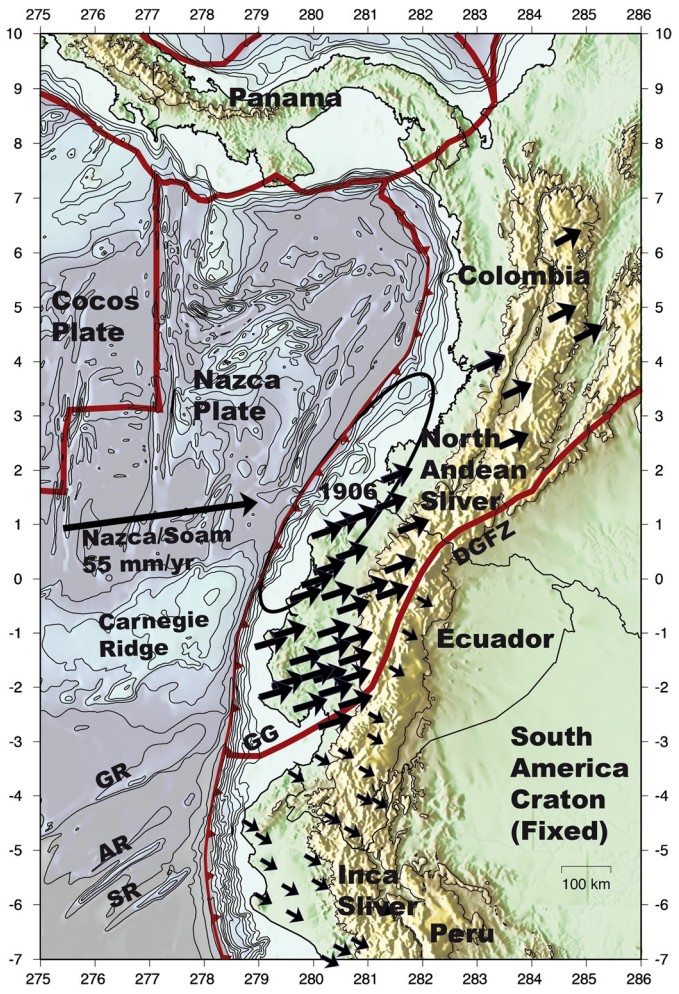

Fig. 1. Seismotectonic setting of the oceanic Nazca plate, South America Craton (SoAm) and two slivers: the North Andean Sliver (NAS) and the Inca Sliver (IS). The relative Nazca/SoAm plate convergence rate in Ecuador is about 55 mm/yr (Kendrick et al., 2003). Black arrows indicate the diverging forearc slivers motions relative to stable SoAm are computed from the pole solutions of Nocquet et al. (2014). The NAS indicates a northeastward long-term rigid motion of about 8.5 ± 1 mm/yr. The ellipse indicates the approximate rupture of the great 1906 Mw = 8.8 Colombia–Ecuador megathrust earthquake. The Carnegie Ridge intersects the trench in central Ecuador and coincides with the southern limit of the great 1906 event. Plate limits (thick red lines) are from Bird (2003). DGFZ = Dolores–Guayaquil Fault Zone; GG = Gulf of Guayaquil; GR = Grijalva Ridge; AR = Alvarado Ridge; SR = Sarmiento Ridge. (For interpretation of the references to color in this figure legend, the reader is referred to the web version of this article.)

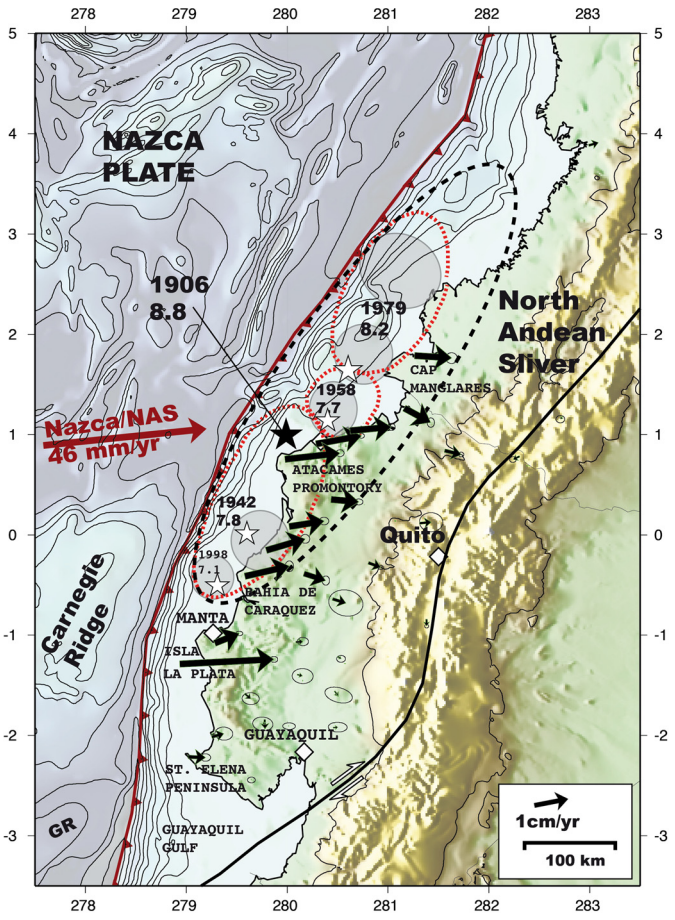

Fig. 2. Interseismic GPS velocity field in the North Andean Sliver reference frame. The relative Nazca/NAS convergence rate is 46 mm/yr. The highest GPS velocity of 26 mm/yr is found on La Plata Island that is the closest point to the trench axis. The GPS network adequately covers the rupture areas of the 1998 Mw = 7.1, 1942 Mw = 7.8 and 1958 Mw = 7.7 earthquakes but only 1/4th of the 1979 Mw = 8.2 and 2/3rd of the great 1906 Mw = 8.8 rupture area. The black star is the epicenter of the great 1906 event and white stars are the epicenters of the Mw > 7.0 1942–1998 seismic sequence. Grey shaded ellipses are the high slip region of the 1942, 1958, 1979 and 1998 seismic sources (Beck and Ruff, 1984; Segovia, 2001; Swenson and Beck, 1996). Red dashed contours are the relocated aftershocks areas of the 1942, 1958 and 1979 events (Mendoza and Dewey, 1984). (For interpretation of the references to color in this figure legend, the reader is referred to the web version of this article.)

the seismic cycle was neglecting subtle transient slip episodes as postseismic after-slip and slow slip events (SSE), the asperity model was an important step forward in our understanding of the earthquake rupture complexities.

Interseismic coupling (ISC) models derived from the inversion of interseismic geodetic data have highlighted a heterogeneous pattern of highly coupled patches separated by creeping patches that is consistent with the concept of the asperity model. Heterogeneous patterns of ISC reflect strong variations in the steady-state fault friction properties with fault zones principally governed by a velocity-weakening behavior (locked asperities), and fault zones that follow a velocity-strengthening behavior (creeping patches) (Hsu et al., 2006; Perfettini et al., 2010; Scholz, 1998). There is growing evidence that the highly coupled patches of ISC models correlate well with the high coseismic slip areas of large earthquake source models (Chlieh et al., 2008; Konca et al., 2008; Loveless and Meade, 2011; Moreno et al., 2010) supporting the persistent character of seismic asperities over the few-years observation period. This correlation implies that ISC models may provide robust framework to build future seismic source scenarios running from the simple static forward models based on the independent failure of each asperity to complex dynamical rupture models involving the simultaneous rupture of several asperities. Creeping patches of ISC models appear also to play an important role in the earthquake segmentation, acting as transient or persistent barriers to the propagation of seismic ruptures. Although, the ability of a creeping barrier to impede or not a seismic rupture is still not very well understood, fundamental characteristics such as the barrier width and its average level of coupling/decoupling appears to be key parameters in controlling their resistance (Kaneko et al., 2010). Dynamic numerical simulations of earthquake sequences based on state and rate friction laws suggest that the slip history and the dynamic weakening due to thermal pressurization can strongly influence the rupture to jump over a creeping barrier and break simultaneously several asperities (Kaneko et al., 2010; Noda and Lapusta, 2013).

A wide diversity of slow slip events (SSEs) has been reported from the Pacific subduction zones including Cascadia,

Alaska, Japan, New Zealand, Mexico and Costa Rica (Schwartz and Rokosky, 2007). Many of these SSEs were observed to occur within the brittle–ductile transition zones, right beneath interseismically locked asperities. These events are called "slow" because of an excessively slow rupture velocity compared to classical earthquakes. SSEs duration can last from days to years with a seismic moment release ranging from many order of magnitude, typically from 10^{11} N m to 10^{20} N m (Table 1 in Ide et al., 2007). SSEs were often documented to be accompanied by tremors, swarms and even moderate Mw $\sim$ 4–6 earthquakes. In all cases, the SSEs moment is always much higher than the cumulative seismic moment, suggesting a process dominated by aseismic slip. Along the Ecuadorian subduction zone, a one-week long SSE was documented in August 2010 beneath La Plata Island (Vallée et al., 2013). The 2010 SSE released a moment equivalent to an Mw = 6.0–6.3 earthquake and triggered intense swarm activity of 650 detected events. The cumulative seismic moment of the 650 events represents only 0.2% of the SSE moment, attesting to a prevailing aseismic process. The synchronous swarms/SSEs activity suggests that previous seismic swarms recorded in the same region of Ecuador during 1 month in 1998 and again in 2002 and 3 months in 2005, might be an indicator of previous much larger SSEs.

Nocquet et al. (2014) proposed a first large-scale analysis of the GPS measurements in North Peru and Ecuador to explain the continental deformation partitioning that is highly controlled by the diverging motion of two continental slivers: the Inca Sliver in Peru and the North Andean Sliver in Ecuador and Colombia (Fig. 1). In this study, we propose to focus on the Ecuadorian subduction zone to evaluate more in detail the degree of locking of the megathrust and compare it with the occurrence of large megathrust earthquakes. We first describe the GPS measurements and dissociate the long-term motion of the North Andean Sliver and the interseismic deformation due to the interplate coupling. The spatial power of slip resolution of the GPS network is explored together with the moment conservation. Then we search for the best family of ISC models that explain the interseismic GPS velocities taking into account the uncertainties of data/models. A model of the 2010 La Plata SSE is also proposed and compared to the interseismic model. Finally, we discuss the implication of the interseismic coupling map regarding the seismic and aseismic slips on the megathrust interface.

2. GPS data and spatial resolution

Data from 100 permanent and campaign GPS stations from Peru, Ecuador and Colombia brings new insight into the geodynamical processes that occur along the north Andes subduction zone. The GPS velocities reveal a complex partitioning between the long-term motion of two diverging slivers, the North Andean Sliver (NAS) and the Inca Sliver, superimposed to signal of the interseismic strain build up caused by the subduction interplate coupling (Nocquet et al., 2014). The NAS extends from the north of the Gulf of Guayaquil to western Venezuela, including the western margin of Ecuador and Colombia (Fig. 1). The secular motion of the NAS can be well explained with an Euler pole located at long. 83.40°W and lat. 15.21°S with an angular velocity $w = 0.287°$/Myr. This pole predicts a northeastward motion of the sliver relative to a stable South America reference frame at a velocity of 7.5 to 9.5 mm/yr. The newly defined kinematic of the NAS accommodates a significant portion of the plate convergence resulting in slower interseismic velocities than previously published in Ecuador and Colombia (Trenkamp et al., 2002; White et al., 2003). In central and northern Ecuador, coastal velocities of 15–25 mm/yr in the South American (SoAm) reference are reduced to 10–15 mm/yr in the NAS reference frame. Similarly, changing from a SoAm to NAS referential reduces the velocity of La Plata Islands (Fig. 2) from 36 mm/yr to 26 mm/yr and the velocity of Salinas in the Santa Elena Peninsula from 15 mm/yr to 5 mm/yr (see comparison in Fig. S1). The resulting relative convergence rate between the Nazca plate and the NAS is 46 mm/yr (Fig. 2). Direct forward 2D models (Fig. S2) done along three profiles in north, central and southern Ecuador (Fig. S1), indicate that the interseismic coupling along the Ecuadorian margin is heterogeneous and decreases southward. It is the highest in north Ecuador where the locked fault zone reaches 30 km depth (Forward models section in the supplementary material).

To study in detail the interseismic coupling, we selected the 30 GPS sites located between the trench and the eastern boundary of the NAS (28 sites in Ecuador and 2 sites in Colombia) from the solution presented by Nocquet et al. (2014). The data set is composed by 16 campaign sites installed since 1994 by the Instituto Geográfico Militar of Ecuador (IGM), 12 permanent stations progressively installed since 2008 by the Instituto Geofisico IG-EPN, some through the Andes Du Nord project, and two stations in southern Colombia operated by the Instituto Geográfico Agustín Codazzi de Colombia (IGAC) (Fig. 2 and Table S1 in the supplementary material). This GPS velocity field provides a dense and homogeneously distributed coverage in Ecuador. In most of the world's subduction zones, the absence or sparse geodetic data at distances less than 100 km from the trench axis prevent any detailed modeling of ISC along the shallowest portion of the megathrust interface (0–25 km depth). This generally hampers our knowledge of shallow slip which could have dramatic consequences in terms of tsunami hazard assessment as attested by the 2011 Mw = 9.0 Tohoku-Oki earthquake. Spatial resolution tests carried out in many subduction zones: Tohoku-Oki, Sumatra–Andaman or Peru–Chile, indicate that locked patches of 100 km $\times$ 100 km or larger near the trench are not resolved from inland geodetic measurements (Chlieh et al., 2008, 2011; Wei et al., 2012). In Ecuador, the coastline is on average less than 75 km from the trench axis and lies on top of the 15–25 km depth contours of the slab interface (Gailler et al., 2007; Graindorge et al., 2004). Our spatial resolution tests indicate that our GPS network can resolve any patch of the megathrust interface larger than 80 km $\times$ 80 km, even if it is located near the trench axis (Fig. S3A). For smaller patches of 60 km $\times$ 60 km, the spatial resolution still remains high inland but starts to degrade near the trench axis north of latitude 0.5°S (Fig. S3B). In southern Ecuador, the spatial resolution remains high everywhere, especially inland where asperities as small as 40 km $\times$ 40 km can be well resolved (Fig. S3C). Model resolution matrix presented in the supplementary material (Fig. S4) supports that within the deployed GPS network, we might be able to detect any locked asperity capable of producing an Mw $>$ 7.0 seismic rupture. In all checkerboard tests, no constraints are put on the final moment. We found that the moment ratio between the input model and the output model is higher than 85%, which indicates a high conservation of the moment. The proximity of the Ecuadorian coastline with the trench axis combined with the spatial distribution of the GPS stations offers an excellent spatial resolution of the slip on the megathrust compared to many other world subduction zones.

3. Inversion method and results

Using a back-slip approach, we perform non-linear inversions of the GPS data based on a stochastic simulated annealing algorithm to determine the interseismic coupling distribution (Chlieh et al., 2011; Savage, 1983). The megathrust interface is meshed into 20 km-diameter point source elements that follow the slab geometry determined by local geologic and seismic data (Font et al., 2013; Gailler et al., 2007; Graindorge et al., 2004; Hayes et al., 2012). All the source points are embedded in elastic half-space and static displacements are computed from the formalism proposed by Xie and

Yao (1989), Ji et al. (2002). The back-slip rake is allowed to fluctuate ±10° from the local average slip vector direction given by the GCMT catalogue (http://www.globalcmt.org/CMTsearch.html). The backslip rate (V_{back}) is bounded by the relative Nazca/NAS long-term plate rate (V_{pl}) of 46 mm/yr. The interseismic coupling (ISC) is defined as $0 \leq V_{back}/V_{pl} \leq 1$. Consequently, an ISC = 1 indicates a full interplate locking and an ISC = 0 means that the plate contact is completely creeping at the plate convergence rate. Sensitivity tests are carried out in the supplementary material to look at the effect of the earth structure and slab geometry. We found that the Earth structure model used in the inversion does not affect the ISC distribution (Fig. S5 and Table S3). The local dip of the slab geometry affects locally the depth of the asperities but the principal pattern of the interseismic coupling does not vary along-strike (Fig. S6).

The misfit between the GPS observations and model predictions is quantified using a weighted root mean square of the residuals (wrms) criterion. The geodetic inversions are driven by the minimization of a cost function (1) that is a weighted quadratic summation of the misfit to the data wrms and two other terms meant to control the roughness of the back-slip distribution and the moment deficit rate M_d for each point source:

$$\text{Cost} = \text{wrms}^2 + \lambda 1\,\text{Dc}^2 + \lambda 2(\text{Mo} - M_d)^2 \quad (1)$$

Dc represents the differences in back-slip rate between adjacent cells and Mo is an a priori moment deficit rate. The smoothing coefficient λ1 distributes the slip equally along-strike and along-dip through Laplacian constraints and λ2 modulates the weight assigned to minimize the final moment deficit rate. We search for the optimal smoothing factors by varying λ1 from 0.01 to 10 and imposing no constraint on the final moment deficit (λ2 = 0). Fig. 3A shows that the best family models are found in the range $0.1 < \lambda 1 < 1.0$. Fig. S7 shows models for λ1 = 0.1 and λ1 = 1.0 and Fig. 4 reports an intermediate solution for λ1 = 0.25. The ISC distributions of these models show three major size asperities: one in southern Ecuador that extends from Santa Elena Peninsula to Isla La Plata, a second one in Central Ecuador from Bahía de Caráquez to the Atacames promontory and finally a third asperity from Esmeraldas to cap Manglares (Fig. 4 and Fig. S7). These very large asperities appear fragmented into two or three sub-asperities in rougher model solutions (compare Fig. 4, Figs. S7A and S7B). The Santa Elena Peninsula–Isla La Plata asperity encompasses a small low coupled asperity off shore the Santa Elena Peninsula where moderate Mw ∼ 6 events occurred in the 20th century and a larger size asperity beneath La Plata Island which is highly coupled and unknown to have generate any Mw > 7.0 events in the past. In the rupture area of the great 1906 Colombia–Ecuador earthquake, the segmentation of the interseismic coupling into smaller locked asperities suggests that the coupling can be interpreted at multiple length scales. Great earthquakes (Mw > 8.5) are the result of the simultaneous rupture of large asperities as the Bahía de Caráquez-Atacames, the Esmeraldas–Manglares and probably a third one in Colombia. The Bahía de Caráquez–Atacames asperity encompasses three minor asperities with the two southern ones that failed individually in 1998 (Mw = 7.1), 1942 (Mw = 7.8) and possibly a third one unbroken beneath the Atacames Promontory. The Esmeraldas–Manglares asperity encompasses two large and highly coupled asperities that ruptured individually in 1958 (Mw = 7.7) and 1979 (Mw = 8.2). Although, the spatial pattern of coupling may vary between these models, it is important to notice that the global moment deficit rate of these models remains close, in the range of 3.1×10^{18} N m/yr (Mw ∼ 6.9) to 3.7×10^{18} N m/yr (Mw ∼ 7.0).

The model uncertainties due to the limited spatial resolution and moment conservation of the GPS network need to be estimated. For that, we run a second series for λ1 = 0.1, 0.25 and 1.0, and with λ2 > 1.0 to control the final moment deficit rate to vary from 2.0×10^{18} N m/yr to 8.0×10^{18} N m/yr, which brackets the moment deficit rates found in previous models. We found that ISC models with a global moment deficit rate ranging from 2.5×10^{18} N m/yr to 4.5×10^{18} N m/yr (Mw ∼ 6.9 to 7.0) fit equally well the GPS data (Fig. 3B). Fig. 5 shows the family of acceptable ISC models, which share some similar characteristics with the solution shown in Fig. 4 and Fig. S3. Particularly, the lateral variation of the down-dip limit of the coupling remains the same reflecting the high resolution of the GPS data to constrain that parameter. Increasing the smoothing tends to average the coupling of neighboring asperities to a single larger one. When the moment deficit rate is increased, the ISC models tend to widen the updip limit of the brittle–ductile zone of each asperity until it reaches the trench axis.

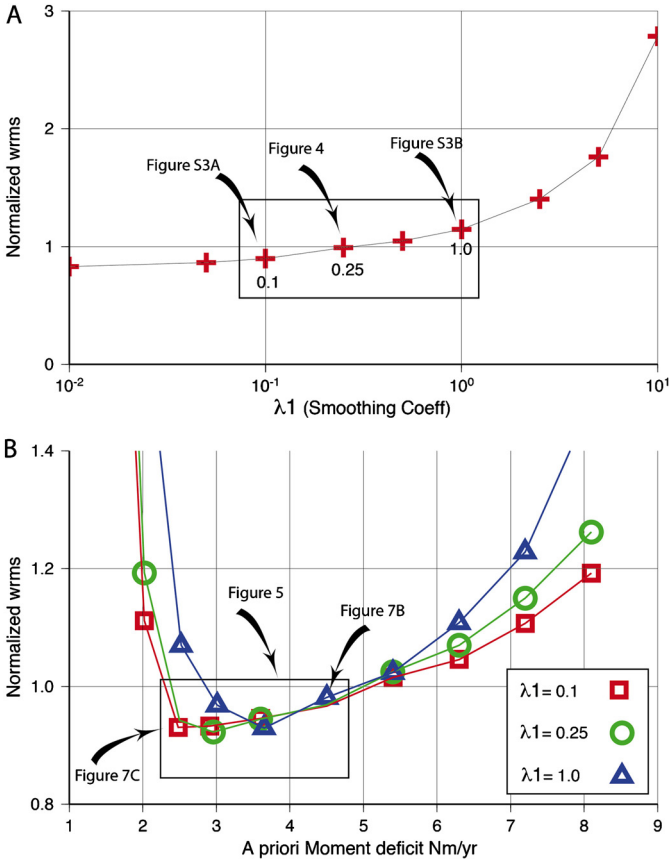

Fig. 3. GPS misfit (normalized wrms) as a function of the smoothing factor coefficient λ1 (A) and of the final moment deficit rate of the model (B). (A) Best family solutions are found for smoothing factors $0.1 < \lambda 1 < 1.0$. In Fig. 4 is reported the solution for λ1 = 0.25 and in Fig. S7, the solutions for λ1 = 0.1 and λ1 = 1.0. (B) The final moment deficit rate is varied for smoothing coefficient λ1 = 0.1, 0.25 and 1.0 and best fitting models are found for final moment deficit rates ranging between 2.5×10^{18} N m/yr and 4.5×10^{18} N m/yr. The ISC distributions of these models are shown in Fig. 5.

4. Discussion

4.1. Slow slip event and interseismic coupling

Below La Plata Island, a circular asperity of about 50 km diameter is found beneath the continental margin toe at less than 15 km depth of the megathrust interface. The presence of this asperity is enigmatic since it does not correspond to any historical large (Mw > 7.0) seismic rupture. Seismic activity near La Plata Island is characterized by frequent swarms that occurred during one

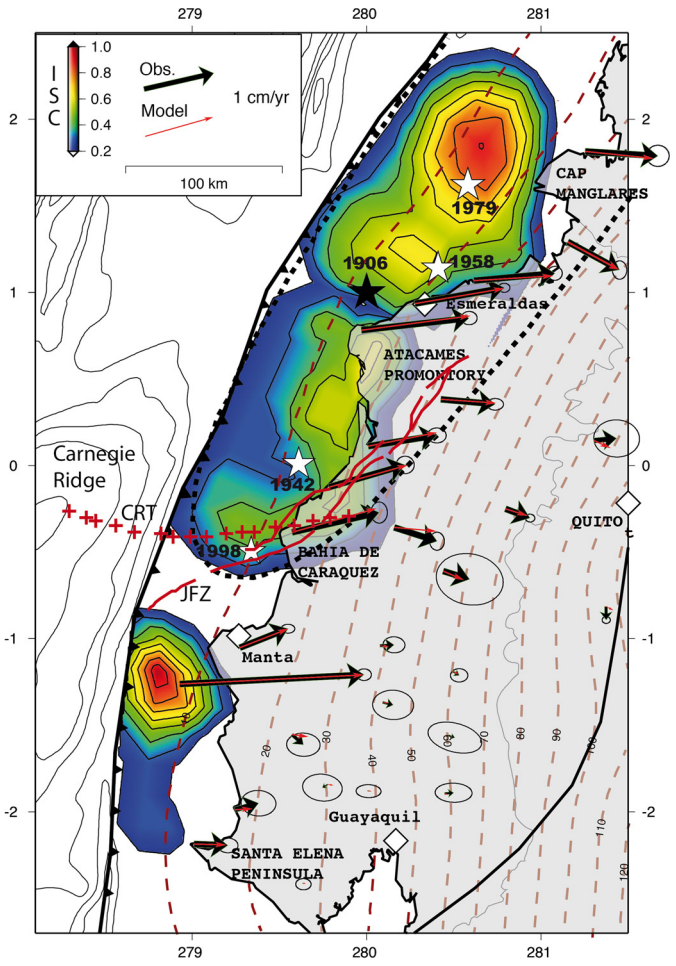

Fig. 4. Distribution of the interseismic coupling (ISC) along the Ecuadorian subduction zone derived from the inversion of the interseismic GPS velocities. The smoothing factor of that solution is $\lambda 1 = 0.25$. No constraint is put on the final moment deficit rate (i.e., $\lambda 2 = 0$). The global moment deficit rate of that solution is $M_d = 3.6 \times 10^{18}$ N m/yr. Red–yellow patches indicate highly locked asperities and white–blue patches the highly creeping regions of the megathrust interface. Arrows represent respectively the interseismic GPS data (black) and synthetic (red). Red dotted lines are the 10-km iso-depth contours of the slab interface (Font et al., 2013). In the rupture area of the great 1906 earthquakes (black dashed line), the coupling is confined within the first 35 km depth of the slab interface. A large creeping corridor lies immediately south of the shallow axis of the Carnegie Ridge Track (CRT) and coincides in map view with the strike-slip Jama-Fault Zone (JFZ) imaged by Multichannel Seismic Reflection (Collot et al., 2004). Southwest of Manta, the permanent GPS station of La Plata Island (ISPT) suggests a highly coupled patch confined between the trench axis and 15-km depth. In south Ecuador, the ISC is weak and shallow. (For interpretation of the references to color in this figure legend, the reader is referred to the web version of this article.)

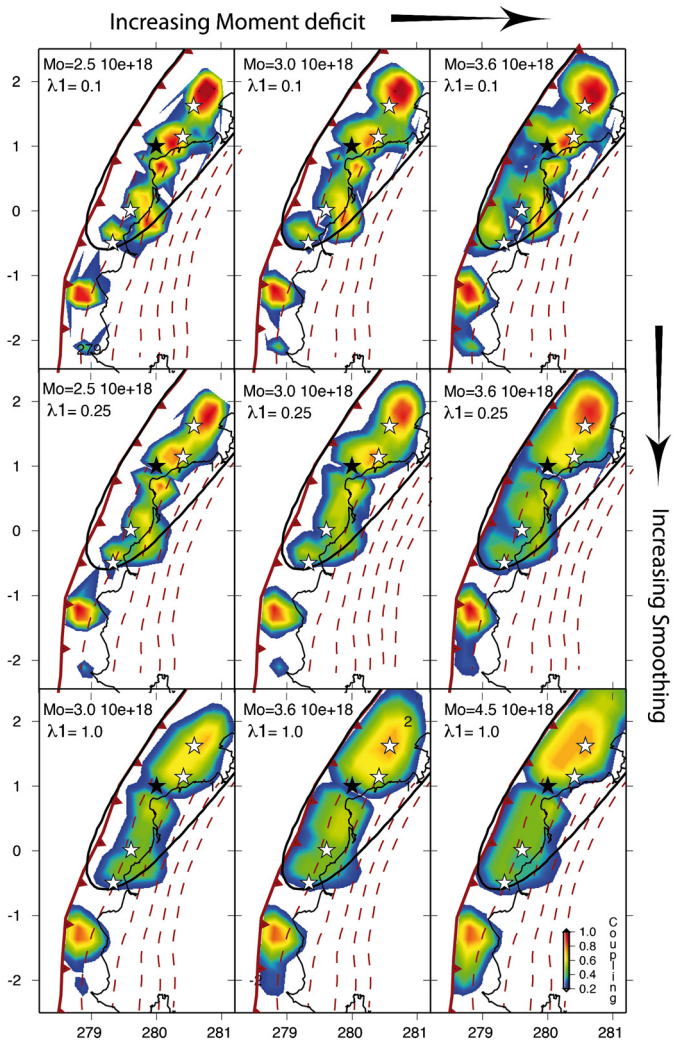

Fig. 5. Best-GPS fitting ISC models for rough ($\lambda 1 = 0.1$, on top), intermediate ($\lambda 1 = 0.25$, middle) and smooth ($\lambda 1 = 1.0$, bottom) solutions. ISC models with a moment deficit rate ranging from 2.5×10^{18} N m/yr to 4.5×10^{18} N m/yr fit relatively well the GPS data and reflect the family of acceptable models (Fig. 3B). The downdip limit of the interseismic coupling does vary between models. Increasing the moment deficit rate extends the updip limit of the coupling near the trench. Rougher solutions evidence the presence of up to seven discrete asperities since smooth solution will tend to local uniform coupling with a maximum of three larger asperities.

month in 1998 and 2002 and three months in 2005 (Segovia, 2009; Vaca et al., 2009). During one week between August and September 2010, a slow slip event triggered intense microseismicity activity near La Plata Island (Vallée et al., 2013). The geodetic signal associated with that SSE was recorded by the permanent GPS station of La Plata Island that suddenly rose ~1 cm and moved ~2 cm westward towards the trench (Fig. 6 and Table S2). The station uplift suggests that the slow-slip occurred either below the island and/or on the deeper portion of the slab interface. Vallée et al. (2013) proposed that a circular slip model centered on La Plata Island with a diameter of 15 km and an average slip of 20 cm fits equally the data than a circle of 32 km diameter with an average slip of 5 cm. Here, we did a slip inversion of that SSE following the same procedure described above and put no constraints on the slip location or final moment. The SSE slip inversion shows that the slip did occur right below La Plata Island overlapping with the asperity and its down dip coupled–uncoupled transition (Fig. 6). The major differences with the models proposed in Vallée et al. (2013), are that the slip occurs over a much wider area of about 50 km diameter or more and that the average slip is much smaller of about 1 cm (with a peak at 2.5 cm). This new slip distribution fits very well with the 3D relocated microseismicity that it triggered (Fig. 6). The 2010 SSE geodetic moment is found to be $Mo = 1.8 \times 10^{18}$ N m, equivalent to an $Mw = 6.1$ earthquake and in good agreement with the moment magnitude range of $Mw = 6.0$–6.3 proposed in Vallée et al. (2013).

Whether such slow slip events release all the stress that is accumulating below La Plata Island is an important question for the seismic hazard in that region. To test this possibility, we compare the along-strike variations of the annual moment deficit of the interseismic model shown in Fig. 4 with the 2010 SSE geodetic moment. Along-strike variations of the moments are computed by averaging along the trench axis the cumulative moment deficit over 20-km wide slab portions (inset of Fig. 6). We found that the 2010 SSE moment is equivalent to 6 months of the annual

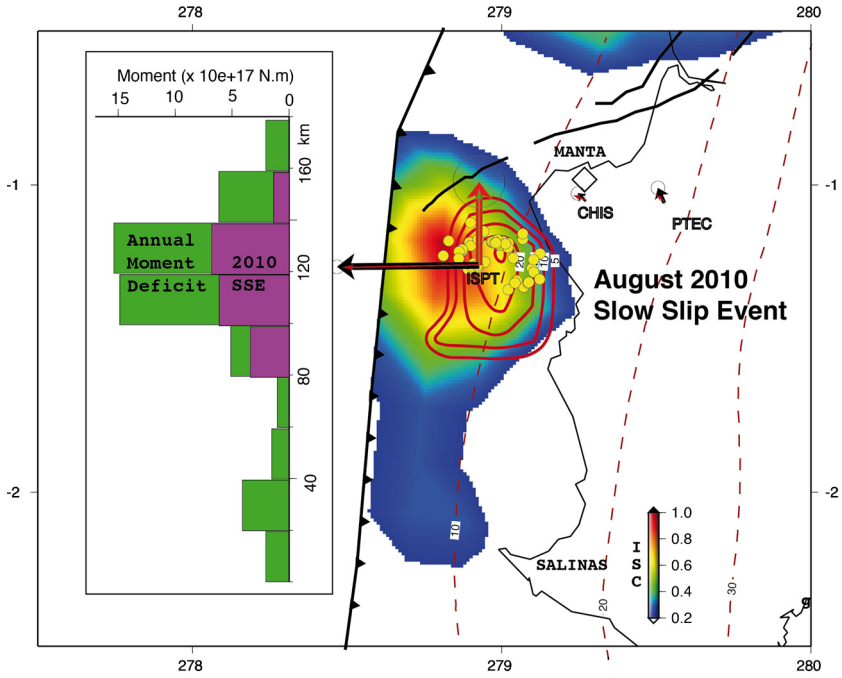

Fig. 6. Slow-slip event of August 2010 below La Plata Island. The 2 cm horizontal and 1 cm vertical GPS motion during that SSE are respectively the black and red thick arrows and synthetics are the thin arrows. The SSE distribution (red contours, each 5-mm) overlaps very well the 3D relocation of the microseismicity (yellow dots) reported by Vallée et al. (2013). The SSE overlaps also the La Plata asperity and its down-dip brittle–ductile transition zone. The 2010 SSE geodetic moment is found to be $Mo = 1.8 \times 10^{18}$ N m, equivalent to the moment magnitude of an $Mw = 6.1$ earthquake. The inset shows a comparison of the along-strike variations of the annual interseismic moment deficit (green) and SSE geodetic moment (purple). Along-strike variations are computed from the moment tensors summation of each cell within 20 km-large slices normal to the trench axis. (For interpretation of the references to color in this figure legend, the reader is referred to the web version of this article.)

interseismic moment deficit. This corresponds to only 10% to 20% of the 5-year cumulative moment deficit since the previous swarm activity in 2005. If we consider the 2010 SSE event as the norm of slow slip event in that region, this would not be efficient enough to release the long-term moment deficit that accumulates on that asperity. At the actual rate of moment deficit, this asperity would accumulate a moment equivalent to an earthquake $Mw = 7.0$ every century and SSEs would contribute to increase that recurrence time only to 110–120 yr. Although still quite debated (Peng and Gomberg, 2010), scaling laws for slow slip events suggest that the equivalent moment release of an SSE scales with its characteristic duration (Ide et al., 2007). This would imply that the individual SSE moment of the 1998, 2002 and 2005 swarm should have been 4 to 12 times larger than that calculated for the 2010 SSE. If so, these four SSEs may have released about 85% of the cumulative moment deficit between 1998 and 2010. This suggests that slow slip events can contribute significantly to release aseismically the interseismic stress and post-pone by a factor of about seven the successive co-seismic failure of La Plata's asperity. At the actual rate of moment deficit, this asperity would accumulate a moment equivalent to an earthquake $Mw = 7.0$ event only every 700 years.

4.2. Segmentation of large and great megathrust earthquakes

The lateral variations in the mechanical properties of the subduction plate interface are believed to be key parameters in the segmentation of large and great megathrust seismic ruptures. The subduction of topographic features such as ridges, fractures zones or seamounts affects these properties and lowers significantly the interplate coupling (Wang and Bilek, 2014). A recent study shows that the rupture limits of thirteen great megathrust earthquakes along the Nazca–South America plate margin are correlated with subducted topography with relief higher than 1000 m (Sparkes et al., 2010). This suggests these geomorphologic features are strong barriers that systematically stop seismic ruptures. The authors also report that the subduction of high seafloor relief creates weak aseismic zones at the plate interface. These weak barriers sometimes prevent propagation of the rupture for large earthquakes but more likely fail during great ($Mw > 8.5$) earthquakes. The characteristics that define strong and weak barriers are still poorly understood, however numerical dynamic simulations of earthquake cycles indicate that the probability for a large earthquake to break through a creeping patch is well correlated with its width and average interseismic coupling level (Kaneko et al., 2010).

In Ecuador, the Carnegie Ridge is the most prominent topographic feature that intersects the trench (Lonsdale, 1978). The northern and southern flanks of that ridge coincide with discrete asperities; one is located below La Plata Island adjacent to the southern flank of the ridge and two are in the rupture areas of the 1998 and 1942 earthquakes, further north (Figs. 4 and 7C). It appears quite clearly in all the ISC models that a large creeping corridor lies immediately south of the shallow axis of the Carnegie Ridge Track (cf. Fig. 11 in Collot et al., 2004) and coincides in map view with a major ENE-trending strike-slip fault, the Jama-Fault Zone (JFZ) imaged by Multichannel Seismic Reflection (Collot et al., 2004). The JFZ cuts the forearc margin from the seafloor to the inter-plate contact, and may contribute to weaken the margin and lower the interseismic coupling on the subduction interface, thus promoting creeping in the corridor (Figs. 4 and 5). That creeping corridor is about 50 ± 10 km long and has an average ISC lower than 0.2, characteristics that may define the behavior of a strong and persistent barrier. This barrier acted as a buffer to all large and great ruptures during the 1906, 1942 and 1998 earthquakes (Fig. 7). Another major barrier appears with a moment deficit rate as low as 0.7×10^{18} N m/yr (km-470 in Fig. 7A) and segment with the Carnegie barrier the megathrust fault in three major asperities (i.e. Santa Elena–La Plata asperity, Bahía de Caráquez–Atacames, Esmeraldas–Manglares; Figs. 4 and 7B). Rougher models indicate that the rupture areas of the 1942, 1958, 1979, 1998 events are separated by weakly coupled segments no larger than about 25 km

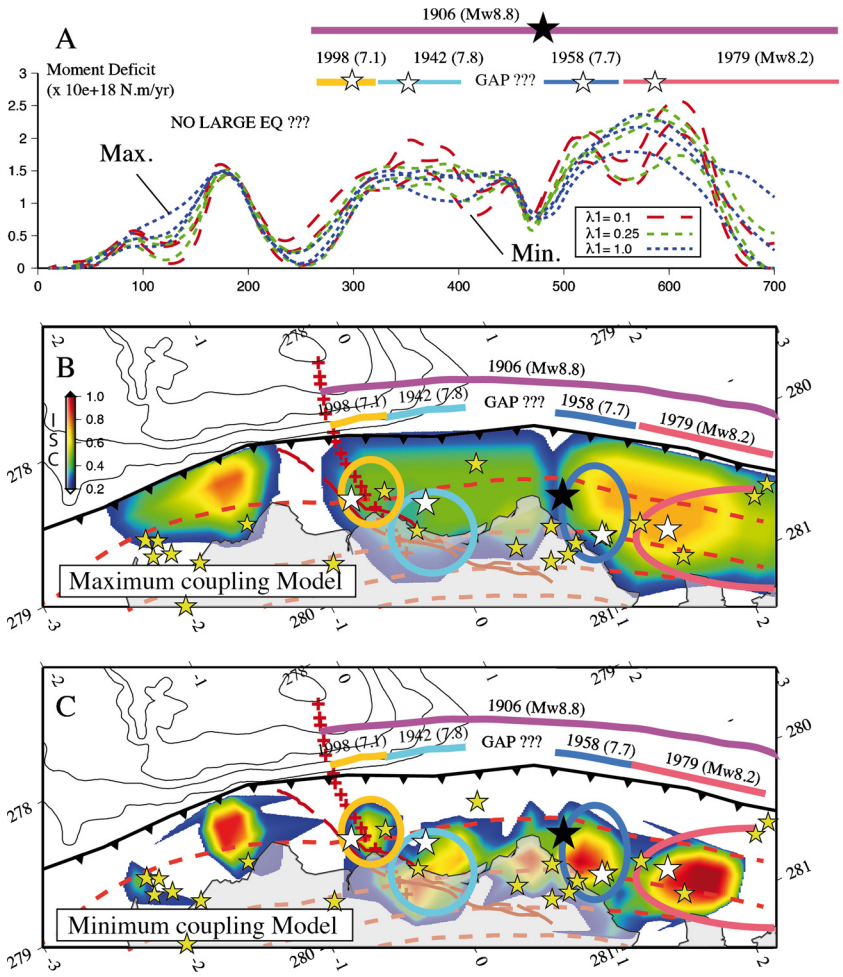

Fig. 7. (A) Along-strike variations of the annual moment deficit for all the interseismic models shown in Fig. 5. (B) Maximum ISC model and (C) Minimum ISC model. (A) The blue, green and red lines correspond to the along-strike variation of the annual moment deficit rate respectively for models with smoothing coefficient $\lambda 1 = 1.0$, 0.25 and 0.1. (B) Smoother solution of Fig. 5 with a maximum moment deficit rate of 4.5×10^{18} N m/yr. (C) Rougher solution of Fig. 5 with a minimum moment deficit rate of 2.5×10^{18} N m/yr. Yellow stars are the epicenters of subduction earthquakes with magnitude Mw > 6.0 from the last 400 yr catalogue (Beauval et al., 2013). (For interpretation of the references to color in this figure legend, the reader is referred to the web version of this article.)

(Figs. 4 and 7C). These segments acted as barriers to the propagation of ruptures. However they probably all failed during the great 1906 earthquake, suggesting that they may have the characteristic of weak barriers with a bi-modal behavior. The size, level of decoupling and lateral spacing of all these barriers determine the along-strike segmentation and bring fundamental characteristics about the potential size and thus magnitude of future large and great megathrust earthquakes along the Ecuadorian subduction zone.

Many local seismic experiments have been conducted in Ecuador providing additional evidence of the segmentation of the subduction margin not only along strike but also along the dip of the slab interface. In map view, mid-crustal seismicity (Font et al., 2013) at the interplate contact occurs around the asperity discretization of the ISC models (Fig. S7). That seismicity is distributed preferentially in the brittle–ductile transition zone of the highly locked asperities but also extends in the creeping patches. Near La Plata Island, the microseismicity underlies very well the down-dip circular shape of that asperity. Microseismicity alignments and clusters appear in ISC regions with values lower than 0.5. The low seismic activity near the trench may suggest an aseismic process there without microseismicity, possibly reflecting the effect of poorly lithified sediments at the toe of the Ecuadorian margin (Collot et al., 2004, 2008; Sage et al., 2006) and its effect on the rheology of the plate interface that promotes stable sliding (Byrne et al., 1988; Scholz, 1998).

4.3. Insights into the sources of historical large megathrust earthquakes

Unless mechanical properties of the megathrust interface vary significantly from one seismic cycle to the other, seismic asperities may be persistent features of the megathrust. The successive rupture of a same subduction segment supports this persistent character. If so, the actual highly locked patches of the ISC models should reveal some characteristics of the seismic asperities that have ruptured during the large historical megathrust earthquakes. We propose here to revisit these past seismic sources in the view of the discrete asperities distributions issue from this study.

The 1906 Mw = 8.8 event

The high heterogeneity of the ISC distribution in the 1906 rupture area brings new insight into historical seismic sources of large megathrust earthquakes along the Ecuadorian margin. The 1906 seismic moment was estimated to be $Mo = 200 \times 10^{20}$ N m (Mw = 8.8) consistent with the estimated tsunami magnitude Mt = 8.7 (Abe, 1979; Kanamori and McNally, 1982). The 500-km long rupture extension was determined from macroseismic reports of severe destructions (Kelleher, 1972) and the epicenter location was determined from the analysis of S–P times from five seismic

stations (Kanamori and McNally, 1982). The rupture extended from 0.5°S where the Carnegie Ridge axis intersects the trench to 4°N at the sharp bend of the northern Colombian trench. Our interseismic GPS data do not resolve the northern portion of the 1906 rupture but it is plausible that the southern limit was stopped by the wide creeping patch found at 0.5°S in all the ISC models (Fig. 5). The great 1906 rupture probably involved the failure of the two very large (or five smaller) asperities found between 0.5°S and 2°N, i.e., the Bahía de Caráquez–Atacames and the Esmeraldas–Manglares asperities (compare Figs. 7B and 7C). Very probably, a third large asperity located offshore Colombia and not resolved by our GPS network did also fail during that great event. In our study area, the largest asperity is found northeast of the 1906 epicenter where the moment deficit rate is about twice higher than in the Central Ecuador (Fig. 7A). This suggests a higher coseismic slip in northern Ecuador and southern Colombia (on the Esmeraldas–Manglares asperity) than in central Ecuador (on the Bahía de Caráquez–Atacames asperity). ISC models suggest also the possibility of shallow coupling confined in the first 20 km depth of the megathrust interface (Figs. 4 and 7B), which are characteristics that may have favored the generation of the 1906 tsunami. The 1906 event shares many similarities with the 2010 Mw = 8.8 Maule earthquake that was also a bi-lateral rupture with a total length of about 550 km. The 2010 Maule coseismic slip peaked around two large asperities with slip up to 13 m and 21 m respectively on the southern and northern asperity at a maximum depth of 40–50 km (Delouis et al., 2010). Probably similar amount of slip or even higher (due to confinement in a narrower zone) should have occurred during the great 1906 Colombia–Ecuador megathrust earthquake.

The 1979 Mw = 8.2 event

The 1979 earthquake was the largest event of the seismic sequence that followed the great 1906 earthquake. It released a moment of Mo = 29×10^{20} N m (Mw = 8.2), equivalent of about 15% of the 1906 seismic moment (Kanamori and McNally, 1982). The rupture initiated in north Ecuador and propagated unilaterally about 240 km northeastward along the Colombian coast. Long-period P wave deconvolution provides a 60 s source time function that exhibits two distinct peaks at 56 and 116 km northeast of the epicenter (Beck and Ruff, 1984), one off-shore the cap Manglares at about 1.8°N and a larger second one at about 3°N. Our ISC models resolve only the location of the southern asperity and indicate that the rupture may have initiated in its southern flank (Figs. 4 and 7C). It appears that the southern limit of the 1979 rupture falls in a 20-km long creeping segment with an ISC ~ 0.4–0.5. This weak and narrow segment separates it from the 1958 asperity and may have played the role of a barrier during that event. The source time function indicates also that the southern and northern asperity released respectively 1/3rd and 2/3rd of the global seismic moment. This may suggest that the interseismic coupling is about twice higher along the northern asperity than along the southern one. However, in absence of coastal GPS stations in Colombia the location, the size and level of coupling of the 1979 northern asperity would still remain elusive.

The 1958 Mw = 7.7 event

The amplitude ratio of the long-period Rayleigh wave of the 1979 and 1958 events suggests a seismic moment for the 1958 earthquake of Mo = 2.8–5.2 × 10^{20} N m (Mw = 7.7). This represents between 10% and 20% of the 1979 seismic moment (Kanamori and McNally, 1982). The rupture length was proposed to be about 50 km (Beck and Ruff, 1984). In that rupture area, the ISC distribution reveals a single circular asperity of 50 km diameter, located north of the city of Esmeraldas at depths of 10–25 km on the slab interface (Figs. 4 and 7C). The 1958 epicenter is located right below that asperity suggesting that the rupture was confined within that single asperity in agreement with its one pulse source time function. The maximum coseismic slip was probably confined between 10 and 20 km depths. It did produce a tsunami associated either with the activation of a spay fault (Collot et al., 2008) or with the deformation of the outer margin wedge (García Cano et al., 2013).

The 1942 Mw = 7.8 event

The source-time function from P-wave analysis of the 1942 earthquake has one simple pulse of moment release with a duration of 24 s suggesting that most of the moment release occurred in a 50-km radius near the epicenter (Swenson and Beck, 1996). The seismic moment of the 1942 event was estimated to be Mo = 6.0–8.0 × 10^{20} N m (Mw = 7.8). The aftershocks affected an elongated region of about 200 km long by 90 km wide parallel to the trench and extending up to 30 km depth (Mendoza and Dewey, 1984). In the ISC model shown in Fig. 4, the 1942 epicenter appears above an elongated area that extends from 1°N to 0.5°S where it is difficult to differentiate discrete asperities. In a rougher ISC solution as shown in Figs. 5 and 7C, the interseismic coupling appears to be fragmented into three smaller asperities disconnected by slightly weaker coupled zone of about 20 km long all with a local average ISC lower than 0.5. The 1942 epicenter is located above the central asperity that crosses the Equator. This asperity extends below the coast at depth of about 20–30 km on the slab interface. If we compare the location of these asperities with the aftershock area defined by Mendoza and Dewey (1984), it is not clear whether only one, two or the three asperities failed during the 1942 earthquake. Some caution should then be exercised in using the aftershock distribution since it over-estimates the coseismic rupture by including both coseismic slip and post-seismic afterslip regions. The 1942 source-time function provides more valuable information with an epicenter location and a rupture extent that is consistent with the location and size of the asperity that crosses the Equator.

The 1998 Mw = 7.1 event

This 1998 Mw = 7.1 earthquake is located offshore the town of Bahía de Caráquez (Fig. 4) at a depth ranging from 25 to 35 km. The focal mechanism obtained from waveform inversion is consistent with a subduction thrust fault event (https://www.geoazur.fr/scardec/scardec_carte.php?carte=Results/Previous_events_of_year_1998/19980804_185920_NearCoastOfEcuador&deep=1; Vallée et al., 2011). This event likely ruptured the asperity right south of the Equator since its source time function presents a single pulse and its epicenter falls right on top of that asperity (Figs. 4 and 7C).

Such a scenario would imply that the asperity found below the Atacames promontory remains unbroken since the 1906 earthquake and can be considered as a seismic gap. The cumulative moment deficit at the actual rate would suggest that it has accumulated a moment deficit equivalent to an Mw = 7.5–7.7 event.

4.4. Characteristic recurrence time of large megathrust earthquakes

It is a critical issue to provide potential information on the recurrence time of such large earthquakes. In term of the asperity model, one possibility is that each asperity has its own characteristic timing and may rupture many times individually before it synchronizes failing with neighboring asperities. Direct observations indicate a recurrence time of 36, 52 and 73 years for the 1942, 1958 and 1979 events respectively after the great 1906 earthquake. Kanamori and McNally (1982) proposed the possibility that the 1942, 1958 and 1979 asperities may fail respectively 6, 4 and 3 times before synchronizing to fail simultaneously in about 210 years, thus generating a great event as that of 1906. If this

hypothesis was true, the 1942 rupture area should have failed in 1978 and the 1958 rupture in 2010 but no similar events occurred suggesting more complexities. Another possibility is to explore the recurrence time for characteristic events and to compare the individual moment deficit rate of each localized asperity with the seismic moments released during past earthquakes. For that, along-strike variations of the annual moment deficit are computed from all ISC models shown in Fig. 5 by averaging along the trench the moment deficit over 20-km large slab slices (Fig. 7A). The moment deficit is integrated along the rupture length of each past earthquake. In the 1942 rupture area, if we suppose that the rupture was confined within the asperity that crosses the Equator (Fig. 7C) and that the 1942 seismic moment was $Mo = 6.0–8.0 \times 10^{20}$ N m, the return time would be of 140 ± 30 yr. Over the rupture area of the 1958 earthquake, if we consider a seismic moment $Mo = 2.8–5.2 \times 10^{20}$ N m, we would find a return time of 90 ± 20 yr. Our model resolves only the southern portion of the 1979 rupture area and uncertainties are much higher for that case. However, if we consider that the coupling along the 1979 rupture area is on average the same than found for the southern asperity, this would suggest a return time of 153 ± 80 yr.

With the actual GPS network, we resolve about 350 km of the 500 km long 1906 rupture. Under the reasonable hypothesis that the ISC is on average the same along the 150 km missing Colombian segment, we find a return time of 575 ± 100 yr. This is in good agreement with the lack of similar great earthquake in the last 400 yr earthquake catalogue (Beauval et al., 2013). One caveat to estimate recurrence time is to consider that the actual moment deficit rates do not vary much during the seismic cycle. A faster moment deficit rate would reduce the return time but this remains elusive with the short time coverage of the actual geodetic measurements.

5. Conclusion

In the last decade, there were a flurry of attempts to predict the nature of strong ground motions and tsunamis that would be generated by the failure of specific seismic gaps. Historical data should be taken with caution to predict future earthquake scenarios because they provide sparse information on the rupture length, width and slip. If seismic asperities are a persistent feature of the megathrust interface, their failure can be better predicted using a discrete asperity description as proposed here. The size, depth and lateral extension of each asperity can be considered as a potential seismic source of future events. The down-dip limit of the asperities that is responsible for strong shaking inland is well resolved in our models. The up-dip limit of the asperities that is a fundamental parameter for tsunami forecasting studies is less well resolved. For that reason, we propose a family of acceptable models including or not slip near the trench within the limits of resolution and uncertainties of the data/models (Figs. 4, 5 and 7). All these parameters should be scaled appropriately for the dimension of the gap, which is expected to break. Seismic scenarios involving the individual or simultaneous rupture of many asperities need to be tested. Scaling laws that link rupture length, width and average displacement can be used to constraint a potential range of acceptable moment magnitude (Leonard, 2010; Wells and Coppersmith, 1994).

The spatial extent, and thus magnitude of future large and great earthquakes is a major issue in seismic hazard. In this study we provide a discrete asperity distribution along the Ecuador coast that brings new insights into the source regions of past and future large megathrust earthquakes in that region. The previous idea that the 1942, 1958 and 1979 ruptures abut each other and cover the complete 1906 rupture area (Kanamori and McNally, 1982; Mendoza and Dewey, 1984; Swenson and Beck, 1996) leaves no space for seismic gaps. This point needs to be reconsidered in the view of our ISC models that suggest that the asperity located between the 1942 and 1958 ruptures, right below the Atacames promontory remains unbroken since the 1906 event (Fig. 7C). A potential for an $Mw > 7.5$ event in the next decades need to be considered there as well as potential tsunami (Ioualalen et al., 2011). Since the 1942, 1958 and 1998 earthquakes broke well localized, individual asperities, the 1979 rupture seems to have involved the rupture of two asperities with only the southern one well resolved by our models. In that framework, the 1906 event may have involved the simultaneous rupture of about two very large (or five small) asperities well described in this study and an additional very large one reported in the 1979 seismic analysis at about 3°N (Beck and Ruff, 1984). The simultaneous rupture of these asperities released a seismic moment five times higher than the sum of the individual seismic moments of the 1942, 1858, 1979, 1998 sequence. This indicates that very large asperities slip much more during great earthquake than during their individual or partial failure. One possible conceptual model of the seismic cycle is that each small asperity has its own characteristic time and its individual failure releases only a partial amount of the moment deficit during large seismic events. The remaining amount being stored to build-up the supercycle event. Only after experiencing several seismic cycles and when many asperities manage to fail together, does a great earthquake occur – corresponding to a supercycle event, thus releasing the remaining moment deficits that have accumulated through many centuries.

Acknowledgements

We thank all the Ecuadorian colleagues of the IG-EPN and IGM for their dedicated work in the field to deploy and maintain the GPS networks. We acknowledge help from the SENESCYT and SENPLADES programs to provide funding for GPS instrumentation and maintenance. L'Agence National pour la Recherche (ANR) from France funded the project "Andes du Nord" (ADN, contract number ANR-07-BLAN-0143-01). This work benefits from the continuous support of the Institut de Recherche pour le Développement (IRD) of France. This work has been carried out in the frame of the Joint International Laboratory 'Séismes & Volcans dans les Andes du Nord'. IRD grant code LMI-SVAN.

Appendix A. Supplementary material

Supplementary material related to this article can be found online at http://dx.doi.org/10.1016/j.epsl.2014.05.027.

References

Abe, K., 1979. Size of the great earthquakes of 1837–1974 inferred from tsunami data. J. Geophys. Res. 84, 1561–1568.

Beauval, C., Yepes, H., Palacios, P., Segovia, M., Alvarado, A., Font, Y., Aguilar, J., Troncoso, L., Vaca, S., 2013. An earthquake catalog for seismic hazard assessment in Ecuador. Bull. Seismol. Soc. Am. 103 (2A), 773–786. http://dx.doi.org/10.1785/0120120270.

Beck, S.L., Ruff, L.J., 1984. The rupture process of the great 1979 Colombia earthquake: evidence for the asperity model. J. Geophys. Res. 89, 9281–9291.

Bird, P., 2003. An updated digital model of plate boundaries. Geochem. Geophys. Geosyst. 4 (3). http://dx.doi.org/10.1029/2001GC000252.

Byrne, D.E., Davis, D.M., Sykes, L.R., 1988. Loci and maximum size of thrust earthquakes and the mechanics of the shallow region of subduction zones. Tectonics 7, 833–857.

Chlieh, M., Avouac, J.P., Sieh, K., Natawidjaja, D.H., Galetzka, J., 2008. Heterogeneous coupling of the Sumatran megathrust constrained by geodetic and paleogeodetic measurements. J. Geophys. Res. 113. http://dx.doi.org/10.1029/2007JB004981. B05305.

Chlieh, M., Perfettini, H., Tavera, H., Avouac, J.-P., Remy, D., Nocquet, J.-M., Rolandone, F., Bondoux, F., Gabalda, G., Bonvalot, S., 2011. Interseismic coupling and seismic potential along the Central Andes subduction zone. J. Geophys. Res. 116. http://dx.doi.org/10.1029/2010JB008166. B1245.

Collot, J.Y., Agudelo, W., Ribodetti, A., Marcaillou, B., 2008. Origin of a crustal splay fault and its relation to the seismogenic zone and underplating at the erosional north Ecuador–south Colombia oceanic margin. J. Geophys. Res. 113. http://dx.doi.org/10.1029/2008JB005691. B12102.

Collot, J.Y., Marcaillou, B., Sage, F., Michaud, F., Agudelo, W., Charvis, P., Graindorge, D., Gutscher, M.A., Spence, G., 2004. Are rupture zone limits of great subduction earthquakes controlled by upper plate structures? Evidence from multichannel seismic reflection data acquired across the northern Ecuador–southwest Colombia margin. J. Geophys. Res. 109. http://dx.doi.org/10.1029/2004JB003060. B11103.

Delouis, B., Nocquet, J.M., Vallée, M., 2010. Slip distribution of the February 27, 2010 Mw = 8.8 Maule Earthquake, central Chile, from static and high-rate GPS, InSAR, and broadband teleseismic data. Geophys. Res. Lett. 37. http://dx.doi.org/10.1029/2010GL043899. L17305.

Font, Y., Segovia, M., Vaca, S., Theunissen, T., 2013. Seismicity patterns along the Ecuadorian subduction zone: new constraints from earthquake location in a 3-D a priori velocity model. Geophys. J. Int. 193 (1), 263–286. http://dx.doi.org/10.1093/gji/ggs083.

Gailler, A., Charvis, P., Flueh, E.R., 2007. Segmentation of the Nazca and South American plates along the Ecuador subduction zone from wide angle seismic profiles. Earth Planet. Sci. Lett. 260 (3–4), 444–464. http://dx.doi.org/10.1016/j.epsl.2007.05.045.

García Cano, L.C., Charvis, P., Galve, A., Marcaillou, B., 2013. 3D velocity structure of the outer forearc of the Colombia–Ecuador subduction zone and implications for the 1958 megathrust earthquake rupture zone. J. Geophys. Res., Solid Earth 119 (2), 1041–1060. http://dx.doi.org/10.1002/2012JB009978.

Graindorge, D., Calahorrano, A., Charvis, P., Collot, J.-Y., Bethoux, N., 2004. Deep structures of the Ecuador convergent margin and the Carnegie Ridge, possible consequence on great earthquakes recurrence interval. Geophys. Res. Lett. 31. http://dx.doi.org/10.1029/2003GL018803. L04603.

Hayes, G.P., Wald, D.J., Johnson, R.L., 2012. Slab1.0: a three-dimensional model of global subduction zone geometries. J. Geophys. Res., Solid Earth 117 (B1). http://dx.doi.org/10.1029/02011JB008524. B01302.

Hsu, Y.-J., Simons, M., Avouac, J.P., Sieh, K., Galetzka, J., Chlieh, M., Bock, Y., Natawidjaja, D.H., Prawirodirdjo, L., 2006. Frictional afterslip following the Mw 8.7, 2005 Nias–Simeuleu earthquake, Sumatra. Science 312 (5782), 1921–1926.

Ide, S., Beroza, G.C., Shelly, D.R., Uchide, T., 2007. A scaling law for slow earthquakes. Nature 447, 76–79. http://dx.doi.org/10.1038/nature05780.

Ioualalen, M., Ratzov, G., Collot, J.Y., Sanclemente, E., 2011. The tsunami signature on a submerged promontory: the case study of the Atacames Promontory, Ecuador. Geophys. J. Int. 184 (2), 680–688. http://dx.doi.org/10.1111/j.1365-246X.2010.04878.x.

Ji, C., Wald, D., Helmberger, D.V., 2002. Source description of the 1999 Hector Mine, California, earthquake, Part I: wavelet domain inversion theory and resolution analysis. Bull. Seismol. Soc. Am. 92 (4), 1192–1207. http://dx.doi.org/10.1785/0120000916.

Kanamori, H., McNally, K.C., 1982. Variable rupture mode of the subduction zone along the Ecuador–Colombia coast. Bull. Seismol. Soc. Am. 72 (4), 1241–1253.

Kaneko, Y., Avouac, J.P., Lapusta, N., 2010. Influence of fault friction heterogeneities on earthquake rupture patterns and interseismic coupling. Nat. Geosci. 3, 363–369. http://dx.doi.org/10.1038/ngeo1843.

Kelleher, J., 1972. Rupture zones of large South American earthquakes and some predictions. J. Geophys. Res. 77, 2087–2103.

Kendrick, E., Bevis, M., Smalley, J.R., Brooks, B., Vargas, R.B., Lauria, E., Souto Fortes, L.P., 2003. The Nazca–South America Euler vector and its rate of change. J. South Am. Earth Sci. 16 (2), 125–131. http://dx.doi.org/10.1016/S0895-9811(03)00028-2.

Konca, A.O., et al., 2008. Partial rupture of a locked patch of the Sumatra megathrust during the 2007 earthquake sequence. Nature 456, 631–635. http://dx.doi.org/10.1038/nature07572.

Lay, T., Astiz, L., Kanamori, H., Christensen, D.H., 1989. Temporal variation of large interplate earthquakes in coupled subduction zones. Phys. Earth Planet. Inter. 54, 258–312.

Leonard, M., 2010. Earthquake fault scaling: self-consistent relating of rupture length, width, average displacement, and moment release. Bull. Seismol. Soc. Am. 100 (5A), 1971–1988. http://dx.doi.org/10.1785/0120090189.

Lonsdale, P., 1978. Ecuadorian subduction system. Am. Assoc. Pet. Geol. Bull. 62 (12), 2454–2477.

Loveless, J.P., Meade, B.J., 2011. Spatial correlation of interseismic coupling and coseismic rupture extent of the 2011 MW = 9.0 Tohoku-oki earthquake. Geophys. Res. Lett. 38 (17). http://dx.doi.org/10.1029/2011GL048561.

Mendoza, C., Dewey, J.W., 1984. Seismicity associated with the great Colombia–Ecuador earthquakes of 1942, 1958 and 1979: implications for barrier models of earthquake rupture. Bull. Seismol. Soc. Am. 74 (2), 577–593.

Moreno, M., Rosenau, M., Oncken, O., 2010. 2010 Maule earthquake slip correlates with pre-seismic locking of Andean subduction zone. Nature 467, 198–202. http://dx.doi.org/10.1038/nature09349.

Nishenko, S.P., 1991. Circum-Pacific seismic potential: 1989–1999. Pure Appl. Geophys. 135, 169–259.

Nocquet, J.-M., Villegas-Lanza, J.C., Chlieh, M., Mothes, P.A., Rolandone, F., Jarrin, P., Cisneros, D., Alvarado, A., Audin, L., Bondoux, F., Martin, X., Font, Y., Régnier, M., Vallée, M., Tran, T., Beauval, C., Maguiña Mendoza, J.M., Martinez, W., Tavera, H., Yepes, H., 2014. Motion of continental slivers and creeping subduction in the northern Andes. Nat. Geosci. 7 (4), 287–291. http://dx.doi.org/10.1038/ngeo2099.

Noda, H., Lapusta, N., 2013. Stable creeping fault segments can become destructive as a result of dynamic weakening. Nature 493 (7433), 518–521. http://dx.doi.org/10.1038/nature11703.

Peng, Z., Gomberg, J., 2010. An integrated perspective of the continuum between earthquakes and slow-slip phenomena. Nat. Geosci. 3 (9), 599–607. http://dx.doi.org/10.1038/ngeo940.

Perfettini, H., Avouac, J.P., Tavera, H., Kositsky, A., Nocquet, J.M., Bondoux, F., Chlieh, M., Sladen, A., Audin, L., Farber, D.L., Soler, P., 2010. Seismic and aseismic slip on the Central Peru megathrust. Nature 465, 78–81. http://dx.doi.org/10.1038/nature09062.

Sage, F., Collot, J.Y., Ranero, C.R., 2006. Interplate patchiness and subduction-erosion mechanisms: evidence from depth migrated seismic images at the central Ecuador convergent margin. Geology 34, 997–1000. http://dx.doi.org/10.1130/G22790A.1.

Savage, J.C., 1983. A dislocation model of strain accumulation and release at a subduction zone. J. Geophys. Res. 88, 4984–4996.

Scholz, C.H., 1998. Earthquakes and friction laws. Nature 391, 37–42.

Schwartz, S.Y., Rokosky, J.M., 2007. Slow slip events and seismic tremor at circum-Pacific subduction zones. Rev. Geophys. 45. RG3004.

Segovia, M., 2001. El sismo de Bahia del 4 de agosto de 1998: caracterizacion del mecanismo de ruptura y analisis de la sismicidad en la zona costera. Tesis de previa a la obtencion del titulo de Ingeniera Geologa thesis. Escuela Politecnica Nacional, Quito, Ecuador. 126 pp. (in Spanish).

Segovia, M., 2009. Análisis espacio-temporal del Enjambre de Puerto López entre enero y febrero de 2005 con observaciones de la estación de banda ancha de OTAVALO. Master thesis. University of Nice Sophia Antipolis, Quito, Ecuador (in Spanish).

Sparkes, R., Tilmann, F., Hovius, N., Hillier, J., 2010. Subducted seafloor relief stops rupture in South American great earthquakes: implications for rupture behaviour in the 2010 Maule, Chile earthquake. Earth Planet. Sci. Lett. 298 (1–2), 89–94. http://dx.doi.org/10.1016/j.epsl.2010.07.029.

Swenson, J.L., Beck, S.L., 1996. Historical 1942 Ecuador and 1942 Peru subduction earthquakes, and earthquake cycles along Colombia–Ecuador and Peru subduction segments. Pure Appl. Geophys. 146 (1), 67–101.

Thatcher, W., 1990. Order and diversity in the modes of Circum-Pacific earthquake recurrence. J. Geophys. Res. 95 (B3), 2609–2623.

Trenkamp, R., Kellogg, J.N., Freymueller, J.T., Mora, H.P., 2002. Wide plate margin deformation, southern Central America and northwestern South America, CASA GPS observations. J. South Am. Earth Sci. 15 (2), 157–171.

Vaca, S., Regnier, M., Bethoux, N., Alvarez, V., Pontoise, B., 2009. Sismicidad de la región de Manta (Ecuador): enjambre sísmico de Manta-2005. In: Geología y Geofísica Marina y Terrestre del Ecuador, Spec. Pub. INOCAR-IRD, pp. 151–166.

Vallée, M., Charléty, J., Ferreira, A.M.G., Delouis, B., Vergoz, J., 2011. SCARDEC: a new technique for the rapid determination of seismic moment magnitude, focal mechanism and source time functions for large earthquakes using body wave deconvolution. Geophys. J. Int. 184, 338–358. http://dx.doi.org/10.1111/j.1365-246X.2010.04836.x.

Vallée, M., Nocquet, J.-M., Battaglia, J., Font, Y., Segovia, M., Régnier, M., Mothes, P., Jarrin, P., Cisneros, D., Vaca, S., Yepes, H., Martin, X., Béthoux, N., Chlieh, M., 2013. Intense interface seismicity triggered by a shallow slow-slip event in the Central-Ecuador subduction zone. J. Geophys. Res. 118, 1–17. http://dx.doi.org/10.1002/jgrb.50216.

Wang, K., Bilek, S.L., 2014. Invited review paper: fault creep caused by subduction of rough seafloor relief. Tectonophysics 610, 1–24.

Wei, S., Graves, R., Helmberger, D., Avouac, J.-P., Jianga, J., 2012. Sources of shaking and flooding during the Tohoku-Oki earthquake: a mixture of rupture styles. Earth Planet. Sci. Lett. 333–334. http://dx.doi.org/10.1016/j.epsl.2012.04.006.

Wells, D.L., Coppersmith, K.J., 1994. New empirical relationships among magnitude, rupture length, rupture width, rupture area, and surface displacement. Bull. Seismol. Soc. Am. 84 (4), 974–1002.

White, S.M., Trenkamp, R., Kellogg, J.N., 2003. Recent crustal deformation and the earthquake cycle along the Ecuador–Colombia subduction zone. Earth Planet. Sci. Lett. 216, 231–242.

Xie, X., Yao, Z.X., 1989. A generalized reflection–transmission coefficient matrix method to calculate static displacement field of a dislocation source in a stratified half space. Chin. J. Geophys. 32, 191–205.